Regular and chaotic orientational and rheological behaviour of liquid crystals

2004 J. Phys.: Condens. Matter 16 S3835

(http://iopscience.iop.org/0953-8984/16/38/005)

INSTITUTE OF PHYSICS PUBLISHING JOURNAL OF PHYSICS: CONDENSED MATTER

J. Phys.: Condens. Matter **16** (2004) S3835–S3859 PII: S0953-8984(04)78582-3

Regular and chaotic orientational and rheological behaviour of liquid crystals

S Hess[1,3] **and M Kröger**[2]

[1] Institut für Theoretische Physik, Technische Universität Berlin, PN 7-1, Hardenbergstraße 36, D-10623 Berlin, Germany
[2] Polymer Physics, ETH Zürich, Wolfgang-Pauli-Straße 10, HCI-537, CH-8093 Zürich, Switzerland

E-mail: s.hess@physik.tu-berlin.de

Received 29 March 2004
Published 10 September 2004
Online at stacks.iop.org/JPhysCM/16/S3835
doi:10.1088/0953-8984/16/38/005

Abstract

The dynamic behaviour of the molecular alignment strongly affects the rheological properties of nematic liquid crystals. The closed nonlinear relaxation equation for the five components of the alignment tensor which was derived within the framework of irreversible thermodynamics and also inferred from a generalized Fokker–Planck equation led to the prediction (Rienäcker *et al* 2002 *Phys. Rev.* E **66** 040702(R); *Physica* A **315** 537) that the rather complex orientational behaviour of tumbling nematics can even be chaotic in a certain range of the relevant control variables. Here the rheological consequences, in particular the shear stress and the normal stress differences, as well as the underlying dynamics of the alignment tensor are computed and discussed. For selected state points, long time averages are evaluated for imposed shear rates. Orientational and rheological properties are presented. The transitions between different dynamic states are detected and discussed. Representative examples of alignment orbits and rheological phase portraits give insight into the dynamic behaviour.

1. Introduction

Nematic liquid crystals subjected to a stationary shear flow can either go to a stationary 'flow aligned state' or have an orientation showing a time dependent, often periodic response. The latter case is referred to as 'tumbling'. Within the Ericksen–Leslie director theory [1–4] this occurs when the 'tumbling parameter', which is the ratio of two viscosity coefficients, is less than one. In general, the orientational dynamics is more complex and requires the tensorial description used here [4–6]. The term 'tumbling nematic' is applied to nematic liquid crystals

[3] Author to whom any correspondence should be addressed.

in the range of temperature or concentration where no stationary flow alignment is obtained for small shear rates. Tumbling has been observed in low molecular weight thermotropic liquid crystals [4, 7], in polymeric main chain liquid crystals [4, 8], as well as in lyotropic liquid crystals and micellar solutions (living polymers) [9, 10]. Even more dramatic is a chaotic behaviour found in theoretical studies [11–13] of the orientational dynamics. It is the purpose of this paper to present results for the rheological behaviour of such a liquid crystal, for a few state points, as a function of the shear rate, as follows from the dynamics of the alignment analysed previously in [11, 13]. At the same time, the theoretical approach is outlined and the applications to flow birefringence, flow alignment, and to the computation of the viscous properties are discussed. Points of departure are coupled equations for the second-rank alignment tensor specifying the orientation of non-spherical particles and for the friction pressure or stress tensor. These equations have been derived from irreversible thermodynamics quite some time ago [5]; for extensions to spatially inhomogeneous systems and for some further extensions, see [14] and [15]. The nonlinear relaxation equation for the alignment tensor has also be derived from a generalized Fokker–Planck equation for the orientational distribution function [6, 16, 17].

Indications for rheo-chaos, i.e., for chaotic rheological behaviour of fluids, have recently been found in experiments [18], and theoretical studies were performed [19], where the underlying dynamics, however, differs from the case studied here. It is hoped that the computations presented will help in the detection of rheo-chaos and identification of its properties for tumbling nematic polymeric and lyotropic liquid crystals, as well as colloidal dispersions of rod-like or disc-like particles and solutions of viruses [20, 21]. For simplicity, liquid crystalline monodomains are treated where the velocity gradient can be considered as an external variable. Treating the full polydomain problem where the hydrodynamic equations for the flow field have to be solved simultaneously with those for the alignment tensor is possible, but computationally more demanding; for first studies of this kind which indicate also the existence of spatial chaos, see [22]. Nevertheless, a detailed analysis of the spatially homogeneous case is needed to find the range of parameters where a regular, stationary or periodic and where a more complex and even chaotic temporal behaviour occur.

Tumbling of isolated ellipsoidal particles in a shear flow was described by Jeffrey over 80 years ago [23]. Within the frame work of the Ericksen–Leslie theory [1], the director specifying the direction of the average orientation in a nematic liquid crystal shows a similar dynamic behaviour or goes to a flow aligned state when the tumbling parameter is below or above 1, respectively [4]. The Ericksen–Leslie theory is a limiting case of the more general tensorial theory when one assumes that the alignment tensor remains uniaxial, as in equilibrium, and that the degree of order is not affected by the flow. For intermediate and large shear rates, however, the biaxiality of the alignment and the change of the order parameter do play a role and the dynamic behaviour of tumbling nematics is far richer than what the Ericksen–Leslie theory can describe. Numerous theoretical studies of the behaviour of nematics in a shear flow, based on a tensorial description and also on the dynamics of the orientational distribution function, have been performed; some key references and reviews are [4–6, 17, 24–31]. The rheological properties in the chaotic regime have not been presented previously.

This paper is organized as follows. In section 2, the basic theory is outlined. The nonlinear relaxation equation for the second-rank alignment tensor is formulated and the constitutive relation for the friction pressure or stress tensor is stated. These equations involve characteristic relaxation time coefficients pertaining to the relaxation of the alignment and to its coupling with the stress tensor or with the velocity gradient. At the same time, the stress contains a contribution associated with the deviation of the alignment from its equilibrium value. Scaled variables are introduced for all physical quantities of interest. The essential model parameters

are, firstly, a temperature or density variable which determines, for an equilibrium situation, whether the system is in an isotropic or nematic state and, secondly, the value of the tumbling parameter which governs whether a stationary or a time dependent response results from a small applied steady shear rate. This quantity, of course, is also an essential control parameter. With the help of five basis tensors, the alignment tensor equation is rewritten in terms of its five components. In the case of a plane Couette flow, three of these components suffice when the alignment has a symmetry in accord with that of the symmetric traceless (deviatoric) part of the velocity gradient tensor. Spontaneous symmetry breaking, however, can occur for certain ranges of parameters. Thus the full set of components is taken into consideration. Similarly, the stress tensor is characterized by five components; the symmetry adapted ones are linked with the shear stress and the first and second normal stress differences. Stress components violating the Couette symmetry can also be non-zero. A brief survey of the nomenclature used to describe the different kinds of stationary states and of symmetry adapted time dependent solutions, such as 'tumbling' and 'wagging', as well as of symmetry breaking ones, such as 'kayaking and tumbling' and 'kayaking and wagging' is given. Section 3 is devoted to a presentation of the rheological properties inferred from time averages of the dynamic equations for selected state points. Graphs are shown for the shear stress and for the viscosity as functions of the shear rate for the isotropic phase, for a shear flow induced transition into the nematic phase, and for a flow aligned nematic. The main emphasis is on a tumbling nematic where, with increasing shear rates, transitions between different dynamic states occur, e.g. from kayaking–tumbling, to tumbling, to kayaking–wagging, to kayaking–tumbling, to a complex and chaotic behaviour, and to a flow aligned state. Graphs of the shear stress and of normal stress differences, as well as of properties of the alignment tensor, give evidence of these transitions. The nature of the dynamic states, however, is more clearly revealed by 'orbits' or 'phase portraits' where components of the alignment tensor are plotted against each other, as well as the first normal stress difference being displayed versus the shear stress. Representative examples of these curves are displayed and discussed in section 4.

2. Relaxation equations and constitutive relations

2.1. The alignment tensor

The alignment of effectively uniaxial particles with a molecular unit vector $\boldsymbol{u}$ is characterized by an orientational distribution function $f(\boldsymbol{u}, t)$ [6, 32–34]. The appropriate order parameter for a nematic is the second-rank alignment tensor

$$\boldsymbol{a} \equiv \sqrt{\tfrac{15}{2}}\langle \overline{\boldsymbol{uu}} \rangle \equiv \int f(\boldsymbol{u}, t)\sqrt{\tfrac{15}{2}}\,\overline{\boldsymbol{uu}}\,\mathrm{d}^2u, \tag{1}$$

which is the anisotropic second moment characterizing the distribution. The symbol $\overline{\boldsymbol{x}}$ indicates the symmetric traceless part of a tensor $\boldsymbol{x}$. Frequently, the alignment tensor is also referred to as a '$\boldsymbol{Q}$-tensor', sometimes as a '$\boldsymbol{S}$-tensor'. The symmetric traceless part of the dielectric tensor which gives rise to birefringence is proportional to the alignment tensor. Thus the shear flow induced modifications of the alignment can be detected optically [35].

For the special case of uniaxial symmetry (uniaxial phase) the alignment tensor $\boldsymbol{a}$ can be parametrized by a scalar order parameter a and the director $\boldsymbol{n}$, i.e., $\boldsymbol{a} = a(3/2)^{1/2}\,\overline{\boldsymbol{nn}}$, such that $a^2 = \boldsymbol{a} : \boldsymbol{a}$ and $-\sqrt{5}/2 \leqslant a = (3/2)^{1/2}\boldsymbol{a} : \overline{\boldsymbol{nn}} \leqslant \sqrt{5}$. The parameter a is therefore proportional to the Maier–Saupe order parameter $S_2 \equiv \langle P_2(\boldsymbol{u}\cdot\boldsymbol{n})\rangle = a/\sqrt{5}$, where P_2 denotes the second Legendre polynomial.

We start by revisiting the underlying original nonlinear relaxation equation for the alignment tensor, based on irreversible thermodynamics. The equation involves characteristic

phenomenological coefficients, namely the relaxation time coefficients $\tau_a > 0$ and τ_{ap}, a dimensionless coefficient (shape factor) κ, the pseudo-critical temperature T^*, the nematic–isotropic transition temperature T_K with $T_K > T^*$, and the positive parameters A_0, B, C (with $C < 2B^2/(9A_0)$) of a Landau–de Gennes potential $\Phi(\boldsymbol{a}) = (1/2)A(T)\boldsymbol{a} : \boldsymbol{a} - (1/3)\sqrt{6}B(\boldsymbol{a}\cdot\boldsymbol{a}) : \boldsymbol{a} + (C/4)(\boldsymbol{a} : \boldsymbol{a})^2$ with $A(T) = A_0(1 - T^*/T)$. The value of A_0 depends on the coefficient of proportionality between $\boldsymbol{a}$ and $\langle \overline{\boldsymbol{uu}} \rangle$ chosen. The choice made in (1) implies $A_0 = 1$; see [5]. The coefficients, on the one hand, are linked with measurable quantities and, on the other hand, can be related to molecular quantities within the framework of a mesoscopic theory [6, 16, 17]. The equation of change for alignment tensor in the presence of a flow field $\boldsymbol{v}$ reads [5, 15]

$$\frac{\partial \boldsymbol{a}}{\partial t} - 2\overline{\boldsymbol{\omega}\times\boldsymbol{a}} - 2\kappa\,\overline{\boldsymbol{\Gamma}\cdot\boldsymbol{a}} + \tau_a^{-1}\boldsymbol{\Phi}(\boldsymbol{a}) = -\sqrt{2}\frac{\tau_{ap}}{\tau_a}\boldsymbol{\Gamma}, \tag{2}$$

where

$$\boldsymbol{\Phi}(\boldsymbol{a}) \equiv \partial\Phi/\partial\boldsymbol{a} = A\boldsymbol{a} - \sqrt{6}B\,\overline{\boldsymbol{a}\cdot\boldsymbol{a}} + C\boldsymbol{a}\boldsymbol{a} : \boldsymbol{a} \tag{3}$$

is symmetric and traceless. The symbols $\boldsymbol{\Gamma}$ and $\boldsymbol{\omega}$ denote the symmetric traceless part of the velocity gradient tensor (strain rate tensor) $\boldsymbol{\Gamma} \equiv \overline{\nabla\boldsymbol{v}}$, and the vorticity $\boldsymbol{\omega} \equiv (\nabla\times\boldsymbol{v})/2$, respectively. In the case of a simple shear flow $\boldsymbol{v} = \dot\gamma y\boldsymbol{e}^x$ in the x-direction, gradient in the y-direction, and vorticity in the z-direction, to be considered throughout the following analysis, these quantities simplify to $\boldsymbol{\Gamma} = \dot\gamma\,\overline{\boldsymbol{e}^x\boldsymbol{e}^y}$ and $\boldsymbol{\omega} = -(1/2)\dot\gamma\boldsymbol{e}^z$. The unit vectors parallel to the coordinate axes are denoted by $\boldsymbol{e}^x$, $\boldsymbol{e}^y$, $\boldsymbol{e}^z$.

Equation (2) has been extended to inhomogeneous systems by changing the time derivative from a partial to a substantial one, and by adding a term $\propto\Delta\boldsymbol{a}$ characterizing inhomogeneous systems [14]; see also [36] for related works. For lyotropic liquid crystals the concentration c of non-spherical particles in a solvent rather than the temperature determines the phase transition; i.e., in this case one has $A \propto (1 - c/c^*)$, where c^* is the pseudo-critical concentration [16]. In [37] similar equations have been used to study the flow alignment and rheology of semi-dilute polymer solutions, where c^* denotes the overlap concentration. In [30] some mathematically rigorous results were obtained using geometric techniques relating to a Landau–de Gennes model of a liquid crystal in a uniform flow. An analysis based on the dynamics of the orientational distribution function is presented in [28]. In [13, 15, 29] the symbol σ was used instead of κ. The special values 0 and ±1 for the coefficient κ in (2) correspond to corotational and codeformational time derivatives. From the solution of the generalized Fokker–Planck equation one finds, for long particles, $\kappa \approx 3/7 \approx 0.4$.

2.2. The pressure tensor

Not only is the alignment influenced by the flow, but also the flow properties as characterized by the friction pressure tensor are affected by the alignment. The full pressure tensor $\boldsymbol{p}$ consists of a hydrostatic pressure p, an antisymmetric part, and the symmetric traceless part $\overline{\boldsymbol{p}}$ referred to as the friction pressure tensor [5]. The latter splits into an 'isotropic' contribution, as already present in fluids composed of spherical particles or in fluids of non-spherical particles in an perfectly 'isotropic state' with zero alignment, and a part explicitly depending on the alignment tensor:

$$\overline{\boldsymbol{p}} = -2\eta_{iso}\boldsymbol{\Gamma} + \overline{\boldsymbol{p}_{al}}, \tag{4}$$

with [15]

$$\overline{\boldsymbol{p}_{al}} = \frac{\rho}{m}k_BT\left(\sqrt{2}\frac{\tau_{ap}}{\tau_a}\boldsymbol{\Phi}(\boldsymbol{a}) - 2\kappa\,\overline{\boldsymbol{a}\cdot\boldsymbol{\Phi}(\boldsymbol{a})}\right). \tag{5}$$

In equilibrium, one has $\Phi(\boldsymbol{a}) = 0$ and consequently $\overline{\boldsymbol{p}_{\rm al}} = 0$. The occurrence of the same coupling coefficient $\tau_{\rm ap}$ in (5) as in (2) is due to an Onsager symmetry relation. For results on the rheological properties in the isotropic and in the nematic phases with stationary flow alignment, following from (2) and (5), see [5, 14, 15, 29]. Here, the main attention is focused on the rheology in the tumbling and in complex dynamic states.

2.3. Scaled variables and model parameters

The equations (2) and (5) can be rewritten in scaled variables [5, 14, 15, 29] which are convenient for the theoretical analysis. At the same time, the essential parameters in the system of differential equations are identified and their physical meaning is discussed. Firstly, the alignment tensor is expressed in units of the value of the order parameter at the isotropic–nematic phase transition:

$$a_{\rm K} = \frac{2B}{3C}, \tag{6}$$

occurring at the temperature $T_{\rm K} > T^*$. With the temperature variable

$$\vartheta \equiv \frac{9}{2}\frac{AC}{B^2} = \frac{1 - T^*/T}{1 - T^*/T_{\rm K}}, \tag{7}$$

the temperature dependence of the uniaxial equilibrium alignment is $a_{\rm eq} = 0$ for $\vartheta \geqslant 9/8$ (isotropic phase) and

$$a_{\rm eq}/a_{\rm K} = \tfrac{1}{4}(3 + \sqrt{9 - 8\vartheta}), \qquad \text{for } \vartheta < 9/8 \text{ (nematic phase).} \tag{8}$$

Notice, that $\vartheta = 1$ corresponds to the equilibrium phase coexistence temperature. The values $\vartheta = 9/8$ and 0 are the upper and lower limits for the metastable nematic and isotropic states, respectively. The quantity $\delta_{\rm K} = 1 - T^*/T_{\rm K}$ which sets a scale for the relative difference of the temperature from the equilibrium phase transition is known from experiments to be of the order 0.1–0.001. On the other hand, it is related to the coefficients occurring in the potential function according to

$$\delta_{\rm K} = \frac{2}{9}\frac{B^2}{A_0 C} = \frac{1}{2}a_{\rm K}^2\frac{C}{A_0}. \tag{9}$$

The derivative $\boldsymbol{\Phi}$ of the potential function in (2) can be written as

$$\boldsymbol{\Phi} = \Phi_{\rm ref}\boldsymbol{\Phi}^*(\boldsymbol{a}^*), \qquad \Phi_{\rm ref} = a_{\rm K}\frac{2}{9}\frac{B^2}{C} = a_{\rm K}\delta_{\rm K}A_0, \quad \boldsymbol{a}^* = \boldsymbol{a}/a_{\rm K},$$

$$\boldsymbol{\Phi}^*(\boldsymbol{a}^*) = \vartheta\boldsymbol{a}^* - 3\sqrt{6}\,\overline{\boldsymbol{a}^* \cdot \boldsymbol{a}^*} + 2\boldsymbol{a}^*\boldsymbol{a}^* : \boldsymbol{a}^*. \tag{10}$$

Clearly, the variable ϑ suffices to characterize the equilibrium behaviour determined by $\boldsymbol{\Phi} = 0$. It should be mentioned that ϑ can be also be interpreted as a density or concentration variable according to $\vartheta = (1-c/c^*)/(1-c_{\rm K}/c^*)$ where c stands for the concentration in lyotropic liquid crystals. For the full nonequilibrium system, times and shear rates are made dimensionless with a convenient reference time. The relaxation time of the alignment in the isotropic phase is $\tau_{\rm a}A_0^{-1}(1 - T^*/T)^{-1}$, showing a pre-transitional increase. This relaxation time, at coexistence temperature $T_{\rm K}$, is used as a reference time:

$$\tau_{\rm ref} = \tau_{\rm a}(1 - T^*/T_{\rm K})^{-1}A_0^{-1} = \tau_{\rm a}\delta_{\rm K}^{-1}A_0^{-1} = \tau_{\rm a}\frac{9C}{2B2} = \tau_{\rm a}a_{\rm K}\Phi_{\rm ref}^{-1}. \tag{11}$$

The shear rates are expressed in units of $\tau_{\rm ref}^{-1}$. The scaled shear rate, a product of the true shear rate and the relevant relaxation time, is also referred to as the 'Deborah number'. Instead of the ratio $\tau_{\rm ap}/\tau_{\rm a}$, the parameter

$$\lambda_{\rm k} = -(2/3)\sqrt{3}\frac{\tau_{\rm ap}}{\tau_{\rm a}}a_{\rm K}^{-1} \tag{12}$$

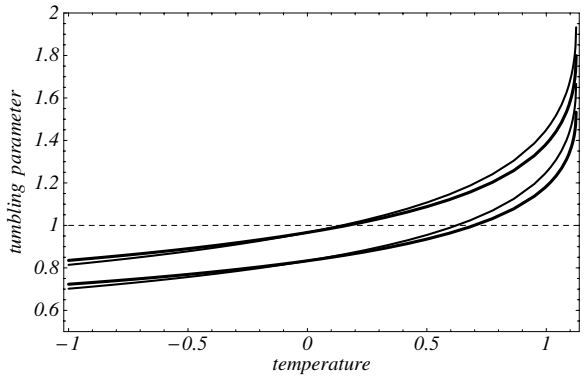

Figure 1. The tumbling parameter as a function of the temperature or concentration variable ϑ for $\lambda_k = 1.45, 1.25$ and $\kappa = 0$ (upper and lower thin curves) as well as $\lambda_k = 1.25, 1.05$ and $\kappa = 0.4$ (upper and lower thick curves). The dashed horizontal line marks the limit between the flow aligned ($\lambda_{eq} > 1$) and the tumbling ($\lambda_{eq} < 1$) states.

is used. As was shown previously [6, 14, 15, 29], the coefficients τ_a and τ_{ap} are proportional to the Ericksen–Leslie [1] viscosity coefficients γ_1 and γ_2, respectively. The present theory applies both for the isotropic and for the nematic phase. The Ericksen–Leslie theory follows from the present approach when the alignment tensor is uniaxial and when the effect of the shear flow on the magnitude of the order parameter can be disregarded. Then it suffices to use a dynamic equation for the 'director' which is a unit vector parallel to the principal axis of the alignment tensor associated with its largest eigenvalue. This is a good approximation deep in the nematic phase and for small shear rates. For intermediate and large shear rates and, in particular, in the vicinity of the isotropic–nematic phase transition, the tensorial description is needed. The 'tumbling coefficient' $\lambda = -\gamma_2/\gamma_1$ is given by

$$\lambda_{eq} = \lambda_k \frac{a_K}{a_{eq}} + \frac{1}{3}\kappa, \tag{13}$$

where a_{eq} is recalled as the equilibrium value of the alignment in the nematic phase. Thus λ_{eq} is equal to λ_k at the transition temperature provided that $\kappa = 0$. Here, the tumbling parameter (13) as a function of temperature is monotonic while some molecular models suggest using a non-monotonic profile. In the limit of small shear rates $\dot\gamma$, the tumbling parameter is related to the Jeffrey tumbling period [23]; see also [29]. A representation of the tumbling parameter in terms of second- and fourth-rank order parameters, which simplifies to the present expression (13) for a simple quadratic closure, has been derived in [38]. Within the Ericksen–Leslie description, the flow alignment angle χ in the nematic phase is determined by

$$\cos(2\chi) = -\gamma_1/\gamma_2 = 1/\lambda_{eq}. \tag{14}$$

A stable flow alignment, at small shear rates, exists for $|\lambda_{eq}| > 1$ only. For $|\lambda_{eq}| < 1$, tumbling and an even more complex time dependent behaviour of the orientation occur. The quantity $|\lambda_{eq}| - 1$ can change sign as a function of the variable ϑ; see figure 1. For $|\lambda_{eq}| < 1$ and in the limit of small shear rates $\dot\gamma$, the Jeffrey tumbling period [23] is related to the Ericksen–Leslie tumbling parameter λ_{eq} by $P_J = 4\pi/(\dot\gamma\sqrt{1-\lambda_{eq}^2})$, for a full rotation of the director.

In the following, both λ_k and κ are considered as model parameters. The first one is essential for the coupling between the alignment and the viscous flow. The second one influences the orientational behaviour quantitatively but does not seem to affect it in a qualitative

way. If one wants to correlate the present theory with the flow behaviour of the alignment in the isotropic phase, on the one hand, and in the nematic phase, on the other hand, for small shear rates where the magnitude of the order parameters is practically unaltered, it suffices to study the case $\lambda_k \neq 0, \kappa = 0$ in order to match an experimental value of λ with the expression (13). Mesoscopic theories [6, 17, 27] indicate that $\kappa \sim \lambda_k$. Thus we also study the case $\kappa \neq 0$, in particular $\kappa = 0.4$. See section 5 for an estimate of model parameters for specific fluids.

2.4. The dimensionless stress tensor

The stress tensor (5) associated with the alignment is related to the relevant quantities expressed in terms of scaled variables by

$$-\overline{\boldsymbol{p}_{\rm al}} = \sqrt{2}\frac{\rho}{m}k_{\rm B}Ta_{\rm K}\Phi_{\rm ref}\frac{\sqrt{3}}{2}\lambda_k\tilde{\boldsymbol{\Phi}}, \qquad \tilde{\boldsymbol{\Phi}} = \boldsymbol{\Phi}^* + \frac{2\kappa}{3\lambda_k}\sqrt{6}\overline{\boldsymbol{a}^*\cdot\boldsymbol{\Phi}^*}, \tag{15}$$

where $\boldsymbol{a}^* = \boldsymbol{a}/a_{\rm K}$ and $\boldsymbol{\Phi}^* = \boldsymbol{\Phi}/\Phi_{\rm ref}$ in (15). The dimensionless shear stress $\boldsymbol{\Sigma}^{\rm al}$ associated with the alignment is defined by

$$\boldsymbol{\Sigma}^{\rm al} \equiv \frac{2}{\sqrt{3}}\lambda_k^{-1}\tilde{\boldsymbol{\Phi}}. \tag{16}$$

Then, equation (15) is equivalent to

$$-\overline{\boldsymbol{p}_{\rm al}} = \sqrt{2}G_{\rm al}\boldsymbol{\Sigma}^{\rm al}, \qquad G_{\rm al} = \frac{3}{4}\frac{\rho k_{\rm B}T}{m}\lambda_k^2\delta_{\rm K}A_0a_{\rm K}^2, \tag{17}$$

where $G_{\rm al}$ is a shear modulus associated with the alignment contribution to the stress tensor, and the product $A_0a_{\rm K}^2$ is essentially one parameter entering the theoretical expressions. The quantity $\eta_{\rm ref} = G_{\rm al}\tau_{\rm al}$ serves as a reference value for the viscosity. With the scaling used here, the dimensionless (first) Newtonian viscosity, in the isotropic phase, is $\eta^*_{\rm New} = 1 + \eta^*_{\rm iso}$ with $\eta^*_{\rm iso} = \eta_{\rm iso}/\eta_{\rm ref}$. For high shear rates the dimensionless viscosity η^* approaches the second Newtonian viscosity $\eta^*_{\rm iso}$. The total deviatoric (symmetric traceless) part of the stress tensor, in units of $G_{\rm al}$, is denoted by $\boldsymbol{\sigma}$. In terms of the quantities introduced here, it is given by (see (4))

$$G_{\rm al}\boldsymbol{\sigma} = -\overline{\boldsymbol{p}} = 2\eta_{\rm iso}\boldsymbol{\Gamma} - \overline{\boldsymbol{p}_{\rm al}} = 2\eta_{\rm iso}\boldsymbol{\Gamma} + \sqrt{2}G_{\rm al}\boldsymbol{\Sigma}^{\rm al}. \tag{18}$$

In the following, we will denote quantities in reduced units by the same symbols as the original ones, unless ambiguities could arise.

2.5. Special geometry and component notation

The symmetric traceless alignment tensor has five independent components. It can be expressed in a standard [39] orthonormalized tensor basis as follows:

$$\begin{aligned} &\boldsymbol{a} = \sum_{k=0}^{4} a_{\rm K}\boldsymbol{T}^k, \qquad \boldsymbol{T}^0 \equiv \sqrt{3/2}\overline{\boldsymbol{e}^z\boldsymbol{e}^z}, \qquad \boldsymbol{T}^1 \equiv \sqrt{1/2}(\boldsymbol{e}^x\boldsymbol{e}^x - \mathbf{e}^y\boldsymbol{e}^y), \\ &\boldsymbol{T}^2 \equiv \sqrt{2}\overline{\boldsymbol{e}^x\boldsymbol{e}^y}, \qquad \boldsymbol{T}^3 \equiv \sqrt{2}\overline{\boldsymbol{e}^x\boldsymbol{e}^z}, \qquad \boldsymbol{T}^4 \equiv \sqrt{2}\overline{\boldsymbol{e}^y\boldsymbol{e}^z}, \end{aligned} \tag{19}$$

where $\boldsymbol{e}^{x,y,z}$ are unit vectors parallel to the coordinate axes. The $\boldsymbol{T}^i$ with $i = 1, \ldots, 5$ are the basis tensors by means of which $\boldsymbol{a}$ is uniquely expressed. The orthogonality relation and the

expression for the coefficients a_K are given by $\boldsymbol{T}^i : \boldsymbol{T}^k = \delta_{ik}$ and $a_K = \boldsymbol{a} : \boldsymbol{T}^k$. Using these basis tensors, from (2) we obtain a system of five ordinary differential equations:

$$\begin{aligned}
\dot{a}_0 &= -\Phi_0 - \tfrac{1}{3}\sqrt{3}\kappa\dot{\gamma}a_2,\\
\dot{a}_1 &= -\Phi_1 + \dot{\gamma}a_2,\\
\dot{a}_2 &= -\Phi_2 - \dot{\gamma}a_1 + \frac{\sqrt{3}}{2}\lambda_k\dot{\gamma} - \frac{1}{3}\sqrt{3}\kappa\dot{\gamma}a_0,\\
\dot{a}_3 &= -\Phi_3 + \tfrac{1}{2}\dot{\gamma}(\kappa+1)a_4,\\
\dot{a}_4 &= -\Phi_4 + \tfrac{1}{2}\dot{\gamma}(\kappa-1)a_3,
\end{aligned} \tag{20}$$

where

$$\begin{aligned}
\Phi_0 &= (\vartheta - 3a_0 + 2a^2)a_0 + 3(a_1^2 + a_2^2) - \tfrac{3}{2}(a_3^2 + a_4^2),\\
\Phi_1 &= (\vartheta + 6a_0 + 2a^2)a_1 - \tfrac{3}{2}\sqrt{3}(a_3^2 - a_4^2),\\
\Phi_2 &= (\vartheta + 6a_0 + 2a^2)a_2 - 3\sqrt{3}a_3a_4,\\
\Phi_3 &= (\vartheta - 3a_0 + 2a^2)a_3 - 3\sqrt{3}(a_1a_3 + a_2a_4),\\
\Phi_4 &= (\vartheta - 3a_0 + 2a^2)a_4 - 3\sqrt{3}(a_2a_3 - a_1a_4),
\end{aligned} \tag{21}$$

and $a^2 \equiv a_0^2 + a_1^2 + a_2^2 + a_3^2 + a_4^2$. The parameters κ, ϑ, λ_k were introduced in the previous section.

The corresponding expansion with respect to the basis tensors and the component notation can be used for the other second-rank irreducible tensors. From equations (16) and (15) one deduces expressions for the (dimensionless) shear stress σ_{xy}, and the normal stress differences $N_1 = \sigma_{xx} - \sigma_{yy}$ and $N_2 = \sigma_{yy} - \sigma_{zz}$ in terms of the dimensionless tensor components $\Sigma_i \equiv \boldsymbol{\Sigma}^{\mathrm{al}} : \boldsymbol{T}^i$, $\phi_i \equiv \boldsymbol{\Phi} : \boldsymbol{T}^i$ and $a_i \equiv \boldsymbol{a} : \boldsymbol{T}^i$. These relations are

$$\sigma_{xy} = \eta_{\mathrm{iso}}\dot{\gamma} + \Sigma_2, \qquad N_1 = 2\Sigma_1, \qquad N_2 = -\sqrt{3}\Sigma_0 - \Sigma_1, \tag{22}$$

with

$$\begin{aligned}
\Sigma_2 &= \frac{2}{\sqrt{3}}\lambda_k^{-1}\left[\phi_2 - \tilde{\kappa}\left(a_2\phi_0 + a_0\phi_2 - \frac{\sqrt{3}}{2}(a_4\phi_3 + a_3\phi_4)\right)\right],\\
\Sigma_1 &= \frac{2}{\sqrt{3}}\lambda_k^{-1}\left[\phi_1 - \tilde{\kappa}\left(a_1\phi_0 + a_0\phi_1 - \frac{\sqrt{3}}{2}(a_3\phi_3 - a_4\phi_4)\right)\right],\\
\Sigma_0 &= \frac{2}{\sqrt{3}}\lambda_k^{-1}\left[\phi_0 - \tilde{\kappa}\left(a_0\phi_0 - a_1\phi_1 - a_2\phi_2 + \frac{1}{2}(a_3\phi_3 + a_4\phi_4)\right)\right],
\end{aligned} \tag{23}$$

and $\tilde{\kappa} = 2\kappa/(3\lambda_k)$.

Expressions for ratios between rheological quantities such as N_2/N_1 or N_1/σ_{xy} are immediately obtained from equations (22), (23).

2.6. Dynamic states

For the following discussions, it is appropriate to review the kinds of dynamic states found from the solution (see [13]) of the differential equations for the components of the alignment tensor:

- Symmetry adapted states with $a_3 = a_4 = 0$:

  Aligning (A): stationary in-plane flow alignment with $a_0 < 0$. Furthermore, one may distinguish states A_+ and A_- pertaining to positive and negative values for the flow alignment angle χ. For nematics composed of rod-like particles the first case occurs for small, the latter one for very large shear rates.

Tumbling (T): in-plane tumbling of the alignment tensor; the main director is in the flow plane and rotates about the vorticity axis.
Wagging (W): in-plane wagging or vibrational motion of the main director about the flow direction.
Log-rolling (L): stationary alignment with $a_1 = a_2 = 0$ and $a_0 > 0$. This out-of-plane solution is unstable, in most cases.

- Symmetry breaking states with $a_3 \neq 0$, $a_4 \neq 0$:

  Stationary symmetry breaking states (SB): which occur in pairs of a_3, a_4 and $-a_3, -a_4$.
  Kayaking–tumbling (KT): the projection of the main director onto the flow plane describes a tumbling motion.
  Kayaking–wagging (KW): a periodic orbit where the projection of the main director onto the flow plane describes a wagging motion.
  Complex (C): complicated motion of the alignment tensor. This includes periodic orbits composed of sequences of KT and KW motion with multiple periodicity as well as aperiodic, erratic orbits. The largest Lyapunov exponent for the latter orbits is positive, i.e., these orbits are *chaotic*.

For a given choice of parameters, in general, only a subset of these solutions are found on increasing the shear rate $\dot{\gamma}$. The T and W states can be distinguished in a plot of a_1 versus a_2. The point $(a_1, a_2) = (0, 0)$ is included in the cycle for tumbling and excluded for wagging. Analogously, in a plot of a_3 versus a_4, the point $(a_3, a_4) = (0, 0)$ is included in the cycle for the KT orbits and excluded for the KW orbits. 'Phase portraits' of this kind are also useful for recognizing more complicated periodic and also irregular orbits; see [13]. Some examples for orbits and phase portraits will be presented later.

The type of orientational behaviour strongly affects the rheological behaviour of the fluid. In the following, rheological properties such as the shear stress, the non-Newtonian viscosity, and the normal stress differences are presented as functions of the shear rate for a few selected values of the temperature and for the other model parameters λ_k and κ. The underlying orientational behaviour is discussed for a few representative cases and we address the question of which rheological properties indicate a chaotic behaviour.

3. Long time and time-averaged rheological behaviour

3.1. The imposed shear rate

In the following, results are presented for the rheological properties calculated from numerical solutions (with a Runge–Kutta method, e.g. via NDSolve of Mathematica™) of the equations (20), (21) governing the dynamics of the alignment and with the expressions (23) for the relevant components of the stress tensor. As initial conditions, a state close to a random orientation is chosen with small (0.01–0.1) but non-zero values for the components of the alignment tensor. Time averages of the components of the alignment tensor and of the stress tensor are evaluated for the relevant range of shear rates. The total run time t_{run} is such that the total shear deformation $\gamma = \dot{\gamma} t_{run} \gg 1$. The desired data are computed as the averages of the values of the tensor components evaluated at time intervals $\Delta t \leqslant 1$. The initial transient behaviour is disregarded, i.e., the data are extracted beginning at times between $t_{run}/3$ and $t_{run}/2$. For those model parameters where a steady state solution exists, stationary solutions are approached rather quickly and the averaging procedure actually would not be needed for long times. In the case of a non-steady response of the alignment, however, the evaluation of

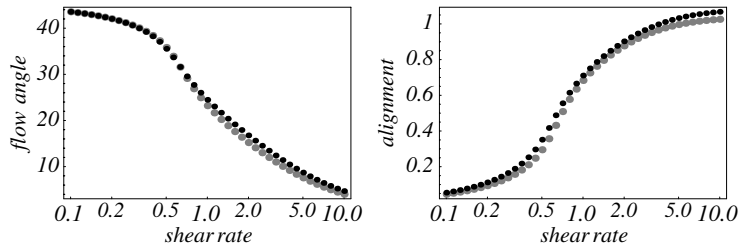

Figure 2. The flow alignment angle and the magnitude of the in-plane alignment as functions of the shear rate for $\lambda_k = 1.25$ and $\kappa = 0$ (black dots) and $\lambda_k = 1.05$ and $\kappa = 0.4$ (grey dots), in the isotropic phase, at the temperature $\vartheta = 2$. The data stem from calculations with constant shear rates, with a maximum shear deformation 150. A logarithmic scale is used for the shear rate.

time averages is essential in order to compare the theory with non-time-resolved rheological measurements where the time average is performed automatically. So it is advantageous to use a method which works in the isotropic phase and for flow aligned as well as for tumbling nematics.

Experiments are not only carried out for imposed shear rates but also for imposed shear stress. Calculations intended to give long time averages for the latter case are performed by replacing the constant shear rate $\dot\gamma$ in (20) by the dynamic shear rate $g = g(t)$ which obeys the equation $\dot g = -(\sigma_{xy}(t) - \sigma_{\rm imp})/(\tau_g \eta_{\rm iso})$. Here σ_{xy} is the instantaneous shear stress as given by (22) with (23), $\sigma_{\rm imp}$ is the imposed constant shear stress, $\eta_{\rm iso}$ is the (second Newtonian) viscosity discussed above, and τ_g is a relaxation time coefficient determining the speed of the shear stress control. Comparison of long time averages from computations with imposed shear stresses and shear rates are presented elsewhere [40]. Here time averages as well as the transient and the dynamic behaviours of the alignment and the stress tensor are analysed for the case of an imposed shear rate.

3.2. Flow alignment and viscosity in the isotropic phase

Results for the flow alignment in the isotropic phase, at the temperature $\vartheta = 2$, are presented in figure 2. The flow angle χ and the magnitude $a_{\rm in} = \sqrt{a_1^2 + a_2^2}$ of the in-plane alignment are displayed as functions of the shear rate. The angle is computed from the relation $\sin(2\chi) = a_2/a_{\rm in}$. The model parameters $\lambda_k = 1.25$, $\kappa = 0$ (black dots) and $\lambda_k = 1.05$, $\kappa = 0.4$ (grey dots) were chosen (see also section 5); the two sets of parameters yield the same value for the tumbling parameter at $\vartheta = 0$. Clearly, in the isotropic phase also there is little difference between the two cases. This is also inferred from the stationary solution of the relaxation equation for the alignment tensor for large ϑ where terms nonlinear in the alignment can be disregarded. In this case one has

$$a_2 = (\sqrt{3}/2)\lambda_k \vartheta^{-1}\dot\gamma \left(1 + (1 - \kappa^2/3)\vartheta^{-2}\dot\gamma^2\right)^{-1}, \tag{24}$$

$$a_1 = \vartheta^{-1}\dot\gamma a_2, \qquad a_0 = -(\sqrt{3}/3)\kappa\vartheta^{-1}\dot\gamma a_2, \tag{25}$$

and $a_3 = a_4 = 0$. The resulting expressions for the angle and the in-plane alignment are

$$\sin(2\chi) = 1/\sqrt{1 + \vartheta^{-2}\dot\gamma^2}, \qquad a_{\rm in} = \sqrt{1 + \vartheta^{-2}\dot\gamma^2}|a_2|. \tag{26}$$

Notice that the expression (26) is independent of λ_k and κ. Thus the small differences seen in the left graph of figure 2 stem from the nonlinear terms in the relaxation equation. The flow angle χ can be determined in a flow birefringence experiment with the incident light beam

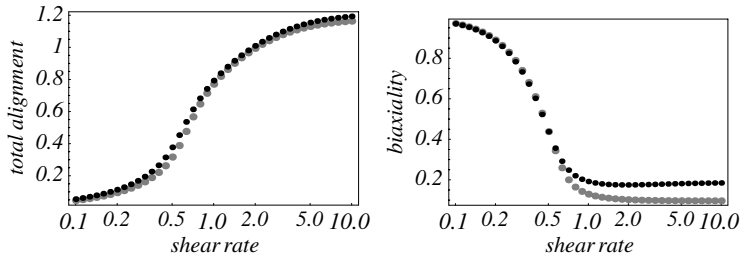

Figure 3. The magnitude of the total alignment and the biaxiality as functions of the shear rate for $\lambda_k = 1.25$ and $\kappa = 0$ (black dots) and $\lambda_k = 1.05$ and $\kappa = 0.4$ (grey dots), in the isotropic phase, at the temperature $\vartheta = 2$. The data stem from calculations with constant shear rates, with a maximum shear deformation 150. A logarithmic scale is used for the shear rate.

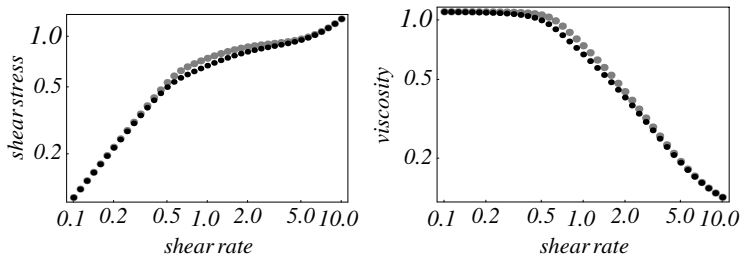

Figure 4. The shear stress (left) and viscosity (right) as functions of the shear rate for $\lambda_k = 1.25$ and $\kappa = 0$ (black dots) and $\lambda_k = 1.05$ and $\kappa = 0.4$ (grey dots), in the isotropic phase, at the temperature $\vartheta = 2$. The data stem from calculations with constant shear rates, with a maximum shear deformation 150. Logarithmic scales are used for both axes.

parallel to the vorticity direction. The birefringence, i.e. the difference $\delta\nu = \nu_1 - \nu_2$ of the indices of refraction ν_1 and ν_2 for light linearly polarized parallel to the in-plane unit vectors $\boldsymbol{e}^1$ and $\boldsymbol{e}^2$ which enclose the angles χ and $\chi + \pi/2$ with the flow direction, is given by

$$2\nu\delta\nu = (15)^{-1/2}(\epsilon_\parallel - \epsilon_\perp)a_K a_{in}\,\mathrm{sgn}(a_2). \tag{27}$$

Here ν is an average index of refraction and $\epsilon_\parallel, \epsilon_\perp$ are the relative electric permeability for electric fields parallel and perpendicular to $\boldsymbol{u}$, assumed to be the optical axis of an effectively uniaxial particle. Measurements of χ as a function of the shear rate, for different values of the temperature or the concentration, in the isotropic phase can be used to determine the reference time needed to scale the shear rates. Similarly, the value of λ_k can be inferred from the birefringence in the small shear rate limit; see section 5.

In figure 3 the magnitude of the total alignment, namely $a = \sqrt{a^2} = \sqrt{a_0^2 + \cdots + a_4^2}$, and the biaxiality parameter b are shown as a function of the shear rate. The latter quantity is inferred from $b^2 = 1 - I_3^2/I_2^3$ where $I_2 = a^2$ and $I_3 = \sqrt{6}\boldsymbol{a} : (\boldsymbol{a} \cdot \boldsymbol{a})$ are the second- and third-order invariants of the alignment tensor. For a planar biaxial alignment as realized for the isotropic phase, subjected to a plane Couette flow with a small shear rate, one has $b = 1$. In a nematic phase in equilibrium, the alignment is uniaxial, which implies $b = 0$. The isotropic fluid subjected to a high shear rate has a small, but non-zero biaxiality. The quantities displayed in figure 3 are practically inaccessible in experiments. The case is different for the shear stress and the normal stress differences to be discussed next.

The shear stress and the viscosity in the isotropic phase are presented in figure 4 as functions of the shear rate. The model parameters are $\lambda_k = 1.25$, $\kappa = 0$ (black dots) and $\lambda_k = 1.05$,

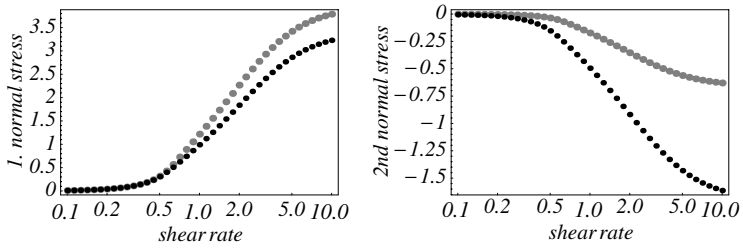

Figure 5. The first and second normal stress differences as functions of the shear rate for $\lambda_k = 1.25$ and $\kappa = 0$ (black dots) and $\lambda_k = 1.05$ and $\kappa = 0.4$ (grey dots), in the isotropic phase, at the temperature $\vartheta = 2$. The data stem from calculations with constant shear rates, with a maximum shear deformation 150. A logarithmic scale is used for the shear rate.

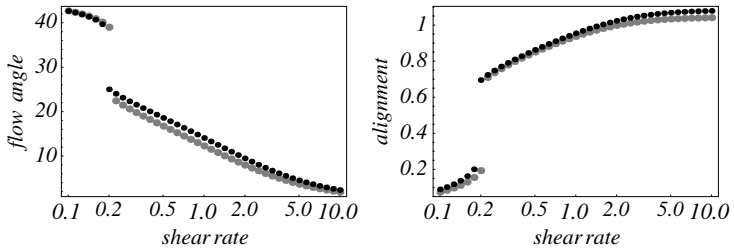

Figure 6. The flow alignment angle and the magnitude of the in-plane alignment as functions of the shear rate for $\lambda_k = 1.25$ and $\kappa = 0$ (black dots) and $\lambda_k = 1.05$ and $\kappa = 0.4$ (grey dots), in the isotropic phase, at the temperature $\vartheta = 1.3$. The data stem from calculations with constant shear rates, with a maximum shear deformation 150. A logarithmic scale is used for the shear rate.

$\kappa = 0.4$ (grey dots), as before. Furthermore, $\eta_{iso} = 0.1$, in reduced units, is chosen. Notice that a double-logarithmic scale is used.

Figure 4, pertaining to the reduced temperature $\vartheta = 2$, shows the behaviour typical for the isotropic phase, namely a first Newtonian viscosity, $\eta = 1.1$ in reduced units for small shear rates, a strong shear thinning for intermediate ones, and the approach to the second Newtonian viscosity $\eta_{iso} = 0.1$ for high shear rates. Calculations with imposed shear rate and imposed shear stress give equivalent results. Again, the two sets of model parameters yield almost identical values for the shear stress and consequently for the viscosity. In contradistinction, differences are quite noticeable for the normal stress differences, in particular for N_2; see figure 5.

3.3. The shear flow induced isotropic-to-nematic phase transition

Still in the isotropic phase, but closer to the phase transition temperature, a shear induced transition to the nematic phase occurs. This is seen in the following figures for $\vartheta = 1.3$ which contain the information on the alignment, the stress, and the viscosity in analogy to the figures shown for $\vartheta = 2.0$.

On the basis of the equations presented here, a shear flow induced isotropic-to-nematic phase transition was predicted theoretically quite some time ago [24, 25]. This phenomenon has been observed in lyotropic liquid crystals, in particular with wormlike micelles [10], and in side chain liquid crystalline polymers [41]. In figures 6–9, results are presented for the same sets of model parameters and for $\vartheta = 1.3$. By comparison, the highest value of ϑ for which a metastable nematic phase exists is $\vartheta = 9/8 = 1.125$. For imposed shear rates, the shear

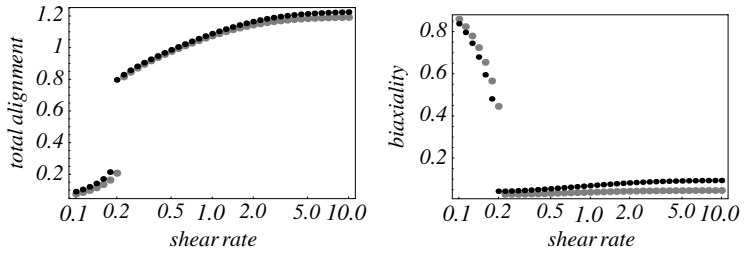

Figure 7. The magnitude of the total alignment and the biaxiality as functions of the shear rate for $\lambda_k = 1.25$ and $\kappa = 0$ (black dots) and $\lambda_k = 1.05$ and $\kappa = 0.4$ (grey dots), in the isotropic phase, at the temperature $\vartheta = 1.3$. The data stem from calculations with constant shear rates, with a maximum shear deformation 150. A logarithmic scale is used for the shear rate.

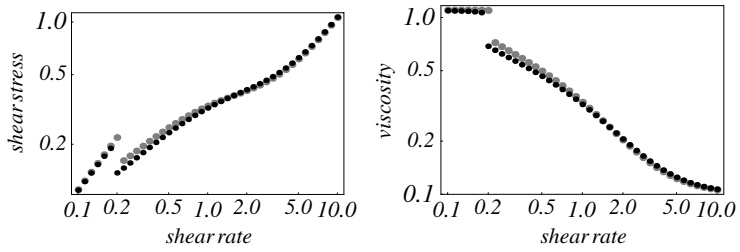

Figure 8. The shear stress (left) and viscosity (right) as functions of the shear rate for $\lambda_k = 1.25$ and $\kappa = 0$ (black dots) and $\lambda_k = 1.05$ and $\kappa = 0.4$ (grey dots), in the isotropic phase, at the temperature $\vartheta = 1.3$. The data stem from calculations with constant shear rates, with a maximum shear deformation 150. Logarithmic scales are used for both axes.

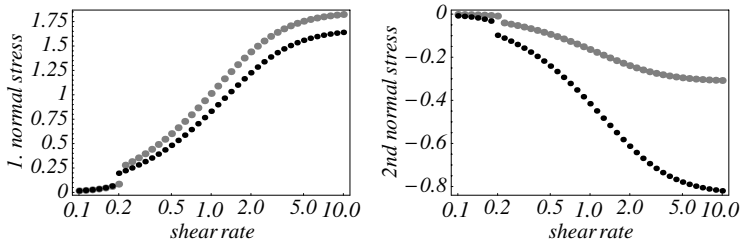

Figure 9. The first and second normal stress differences as functions of the shear rate for $\lambda_k = 1.25$ and $\kappa = 0$ (black dots) and $\lambda_k = 1.05$ and $\kappa = 0.4$ (grey dots), in the isotropic phase, at the temperature $\vartheta = 1.3$. The data stem from calculations with constant shear rates, with a maximum shear deformation 150. A logarithmic scale is used for the shear rate.

stress and consequently the viscosity jump to smaller values at the induced phase transition. For imposed shear stress there is a jump to higher shear rates. Notice the dramatic decrease of the viscosity at the transition and the small biaxiality in the flow induced nematic state, very similar to the small biaxiality in a flow aligned nematic state.

3.4. The flow aligned nematic

For the set of model parameters λ_k and κ, the tumbling parameter (13) is larger than 1 in the temperature or concentration interval $\approx 0.6 < \vartheta < 1.125$; see figure 1. In the range $\approx 0.6 < \vartheta < 1.0$, the solution of the relaxation equation for the alignment tensor, in the

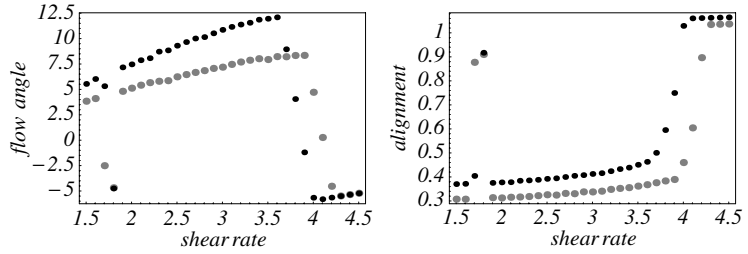

Figure 10. The flow alignment angle and the magnitude of the in-plane alignment as functions of the shear rate for $\lambda_k = 1.25$ and $\kappa = 0$ (black dots) and $\lambda_k = 1.05$ and $\kappa = 0.4$ (grey dots), in the isotropic phase, at the temperature $\vartheta = 0, 0$. The data stem from calculations with constant shear rates, with a maximum shear deformation 750.

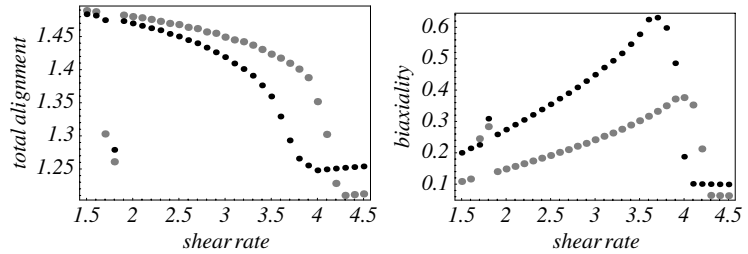

Figure 11. The magnitude of the total alignment and the biaxiality as functions of the shear rate for $\lambda_k = 1.25$ and $\kappa = 0$ (black dots) and $\lambda_k = 1.05$ and $\kappa = 0.4$ (grey dots), in the nematic phase, at the temperature $\vartheta = 0$. The data stem from calculations with constant shear rates, with a maximum shear deformation 750.

presence of a steady shear flow, approaches a flow aligned state. The symmetry breaking components relax to zero, just as in the isotropic phase. In the limit of small shear rates, the magnitude of the alignment is practically unaffected by the flow and the alignment practically remains uniaxial as in equilibrium. In this limiting case, the Ericksen–Leslie theory is applicable; see also [15]. For sake of brevity, no graphs analogous to the previous ones are presented for the flow oriented state; we focus our attention instead on the tumbling regime.

3.5. The tumbling nematic

3.5.1. Survey. Next, results are presented for the time-averaged alignment and for the time-averaged rheological behaviour in the nematic phase at a state point where no stable flow alignment is possible. In particular, the temperature $\vartheta = 0$ and the two sets of parameters $\lambda_k = 1.25, \kappa = 0$ and $\lambda_k = 1.25, \kappa = 0.4$ are chosen again. In figures 10, 11, the flow angle χ, the magnitude of the in-plane alignment a_{in}, the magnitude of the total alignment a, and the biaxiality coefficient b are displayed as functions of the shear rate, in the range $1.5 < \dot{\gamma} < 4.5$, now with a linear scale. Similar to the isotropic phase case, the flow angle χ is determined according to $\sin(2\chi) = a_2/(a_1^2 + a_2^2)(1/2)$ where it is understood that the time-averaged components of the alignment tensor are used. The quantity b, on the other hand, is the time average of the instantaneous biaxiality. The indicators for the alignment show strong variations, even transition-like discontinuities and sign changes in the shear rate intervals between approximately 1.6 and 1.9, and between 3.6 and 4.1. The same feature is seen in plots of the rheological properties displayed in figures 12, 13.

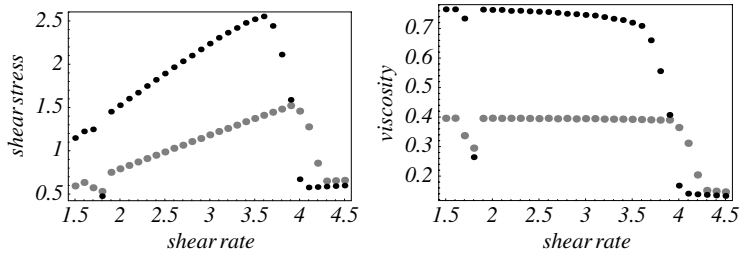

Figure 12. The shear stress (left) and viscosity (right) as functions of the shear rate for $\lambda_k = 1.25$ and $\kappa = 0$ (black dots) and $\lambda_k = 1.05$ and $\kappa = 0.4$ (grey dots), in the nematic phase, at the temperature $\vartheta = 0$. The data stem from calculations with constant shear rates, with a maximum shear deformation 750. Linear scales are used for both axes.

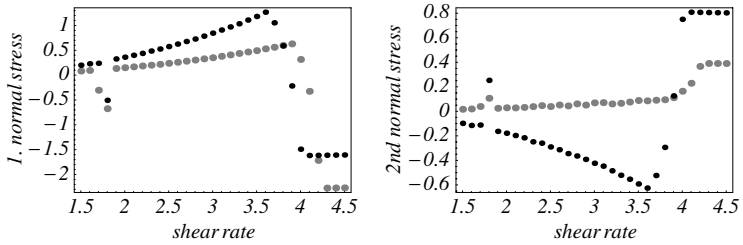

Figure 13. The first and second normal stress differences as functions of the shear rate for $\lambda_k = 1.25$ and $\kappa = 0$ (black dots) and $\lambda_k = 1.05$ and $\kappa = 0.4$ (grey dots), in the nematic phase, at the temperature $\vartheta = 0$. The data stem from calculations with constant shear rates, with a maximum shear deformation 750.

The shear rate intervals where the strong variations occur deserve closer attention. As will be pointed out later, there are transitions between different types of periodic behaviour in the first of these shear rate ranges; in the second one, an irregular chaotic behaviour is found. Despite the noticeable quantitative difference between the data points pertaining to the two sets of model parameters, the qualitative behaviours are rather similar. So the following analysis is restricted to the case $\lambda_k = 1.25$, $\kappa = 0$.

3.5.2. Transitions between dynamic states. In figures 14, 15 the time-averaged flow angle, the magnitude of the in-plane alignment, the shear stress, and the first normal stress difference are displayed. The enhanced resolution of the shear rate clearly reveals that the few points off the curve in the previous figures are not the computational 'measuring errors'. There do indeed relate to transitions between different dynamic states when the shear rate is changed.

Notice the twofold change of sign of N_1, namely from positive to negative to positive, a phenomenon which was observed with main chain polymeric liquid crystals [8]. The flow angle shows a similar behaviour. From figures 14, 15 one might guess that two transitions occur in the interval of shear rates considered. Inspection of figure 16, however, reveals that the sequence of transitions is more complicated. The quantities looked at here are the magnitude of the symmetry breaking or 'out-of-plane' components, namely $\sqrt{a_3^2 + a_4^2}$, and the biaxiality coefficient b. More precisely, the time averages of a_3 and a_4 are squared and added in the evaluation of the magnitude of the 'out-of-plane' components. This quantity is small, but definitely non-zero for $\dot\gamma < 1.68$; it is zero for $1.69 < \dot\gamma < 1.8$, it is large for $1.8 < \dot\gamma < 1.82$, and again small but non-zero for $1.83 < \dot\gamma$. A closer inspection of the orbits—examples are

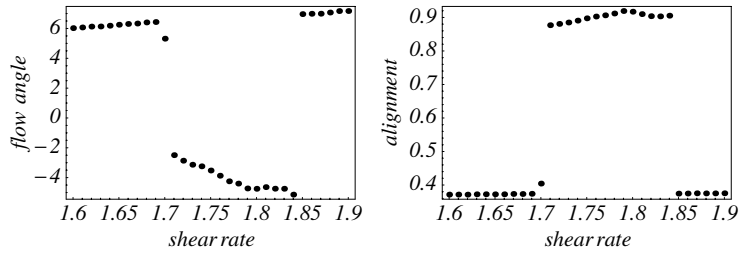

Figure 14. The time-averaged flow alignment angle and the magnitude of the in-plane alignment as functions of the shear rate, in the interval from 1.6 to 1.9, for $\lambda_k = 1.25$ and $\kappa = 0$, in the nematic phase, at the temperature $\vartheta = 0$. The data stem from calculations with constant shear rates, with a maximum shear deformation 750.

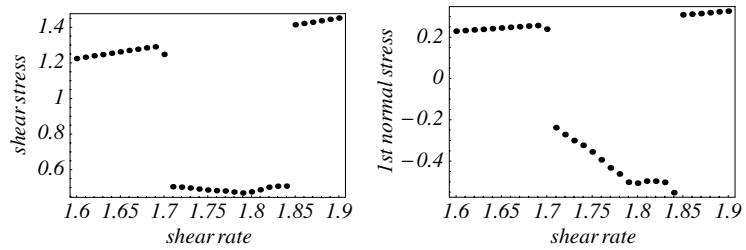

Figure 15. The shear stress and the first normal stress difference as functions of the shear rate for $\lambda_k = 1.25$ and $\kappa = 0$, in the nematic phase, at the temperature $\vartheta = 0$. The data stem from calculations with constant shear rates, with a maximum shear deformation 750.

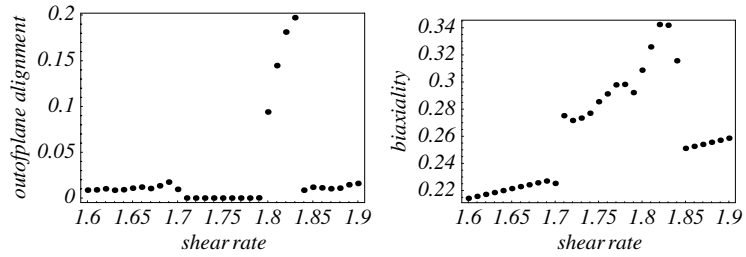

Figure 16. The magnitude of the symmetry breaking components of the alignment tensor and the biaxiality parameter as functions of the shear rate for $\lambda_k = 1.25$ and $\kappa = 0$, in the nematic phase, at the temperature $\vartheta = 0$. The data stem from calculations with constant shear rates, with a maximum shear deformation 750.

given later—indicates the sequence of dynamic transitions KT $\rightarrow$ T $\rightarrow$ KW $\rightarrow$ KT in the range of shear rates considered here.

3.5.3. The chaotic domain. The time-averaged flow angle, the magnitude of the in-plane alignment, the shear stress, and the first normal stress difference for shear rates between 3.6 and 4.1 are displayed in figures 17, 18. A rather irregular behaviour, i.e. a sensitive dependence on the value of the imposed shear rate, is seen. This is indicative of a chaotic behaviour. Indeed, the computation of Lyapunov exponents revealed that the largest one is positive for shear rates in intervals which have a rather fractal character [13]. Also, rather complex periodic orbits

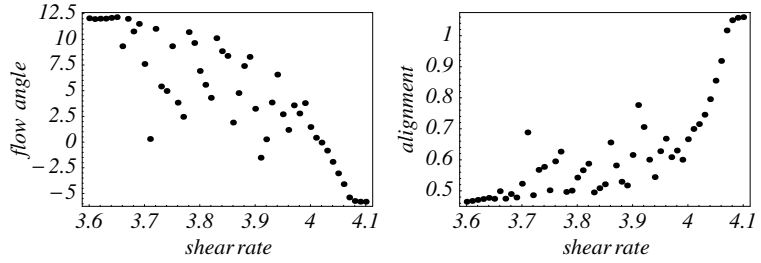

Figure 17. The time-averaged flow alignment angle and the magnitude of the in-plane alignment as functions of the shear rate, in the interval from 3.6 to 4.1, for $\lambda_k = 1.25$ and $\kappa = 0$, in the nematic phase, at the temperature $\vartheta = 0$. The data stem from calculations with constant shear rates, with a maximum shear deformation 1500.

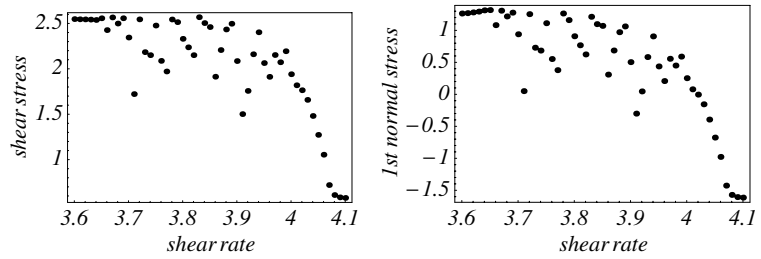

Figure 18. The shear stress and the first normal stress difference as functions of the shear rate for $\lambda_k = 1.25$ and $\kappa = 0$, in the nematic phase, at the temperature $\vartheta = 0$. The data stem from calculations with constant shear rates, with a maximum shear deformation 1500.

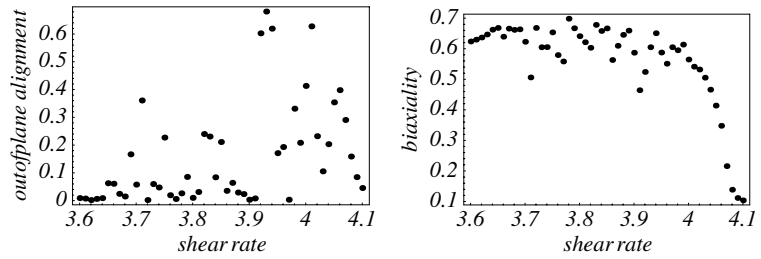

Figure 19. The magnitude of the symmetry breaking components of the alignment tensor and the biaxiality parameter as functions of the shear rate for $\lambda_k = 1.25$ and $\kappa = 0$, in the nematic phase, at the temperature $\vartheta = 0$. The data stem from calculations with constant shear rates, with a maximum shear deformation 1500.

were observed [13]. Notice that the first normal stress difference and the average flow angle are positive for $\dot{\gamma} < 4.0$ and negative for $\dot{\gamma} > 4.0$. A smooth, curve-like dependence on the shear rate is found for $\dot{\gamma} > 4.1$ where a flow aligned state is reached.

The magnitudes of the symmetry breaking components of the alignment tensor and the biaxiality coefficient as displayed in figure 19 for the same range of shear rates also show a rather erratic dependence on the shear rate. Notice the strong decrease of the biaxiality towards the flow aligned state at the higher shear rates.

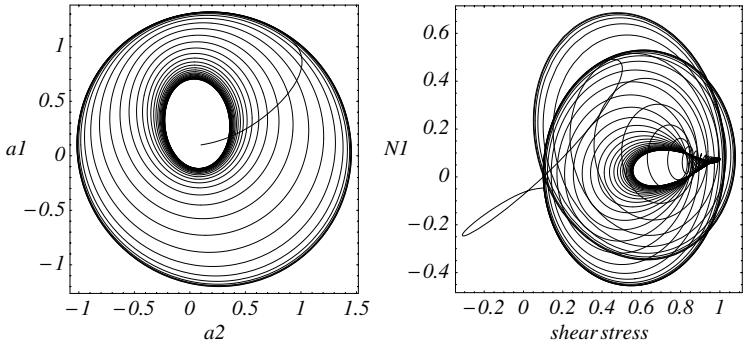

Figure 20. The in-plane orbit a_1 versus a_2 and the rheological phase portrait, namely the normal stress difference N_1 versus the shear stress in the kayaking–tumbling regime, at the shear rate 1.0 with the maximum shear deformation 400. The temperature is $\vartheta = 0$; the model parameters are $\lambda_k = 1.25$ and $\kappa = 0$.

4. Orbits

4.1. General remarks; the flow aligned state

Instead of analysing the components of the alignment and stress tensors as functions of the time, it is more instructive to produce 'orbits' or 'phase portraits' where one component is plotted versus another one. The true alignment orbit is a curve in five-dimensional space; the two-dimensional orbits to be shown are projections on various planes. Usually, the notion 'phase portrait' is applied to plots of a 'velocity' (time derivative) versus a 'coordinate'. Here a plot of a normal stress difference versus the shear stress is referred to as a 'rheological phase portrait'. In a stationary state, the alignment orbits consist of a single point; relatively simple curves indicate the transient behaviour during the approach towards the asymptotic state. The symmetry adapted components a_0, a_1, a_2 of the alignment tensor as well as the shear stress and the normal stress differences approach single non-zero values, whereas the symmetry breaking components a_3, a_4 tend to zero. The orbits look drastically different for periodic and for the chaotic solutions to be presented next, in an order as encountered with increasing shear rates, at $\vartheta = 0$. All orbits to be shown start from the initial values $-0.1, 0.1, 0.1, 0.1, -0.1$ for $a_0, \ldots, a_4$.

4.2. Kayaking and tumbling

As already mentioned above, for $\lambda_k = 1.25$, $\kappa = 0$, and $\vartheta = 0$, periodic solutions of KT type are found for shear rates below $\approx$1.68 as well as between 1.83 and about 3.65. Typical orbits and rheological phase portraits are shown in figures 20, 21 for $\dot\gamma = 1.0$. Limit cycles are approached after a relatively long and complex transient behaviour. The instantaneous magnitudes of the symmetry breaking components a_3 and a_4 can be rather large. Their time averages, however, are relatively small since these quantities are approximately symmetric about zero. The case is different for the KW solutions to be discussed later.

4.3. In-plane tumbling

In-plane tumbling solutions occur for shear rates between approximately 1.7 and 1.8, for the same model parameters as above. Typical orbits, analogous to the previous ones, are shown in figures 22, 23 for $\dot\gamma = 1.75$. Notice that the symmetry breaking components of the

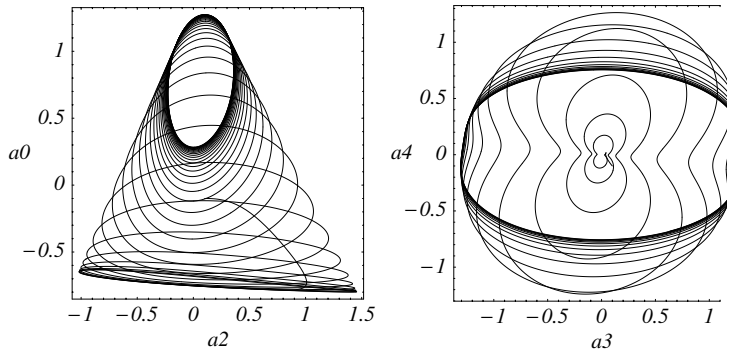

Figure 21. The orbit a_0 versus a_2 and the symmetry breaking orbit a_4 versus a_3 in the kayaking–tumbling regime, at the shear rate 1.0 with the maximum shear deformation 400. The temperature is $\vartheta = 0$; the model parameters are $\lambda_k = 1.25$ and $\kappa = 0$.

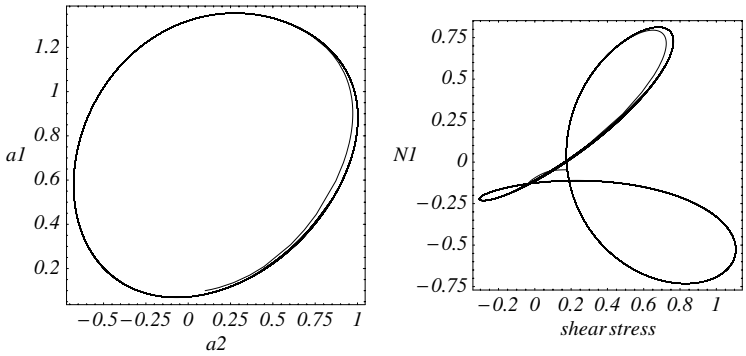

Figure 22. The in-plane orbit a_1 versus a_2 and the rheological phase portrait, namely the normal stress difference N_1 versus the shear stress in the in-plane tumbling regime, at the shear rate 1.75 with the maximum shear deformation 1750. The temperature is $\vartheta = 0$; the model parameters are $\lambda_k = 1.25$ and $\kappa = 0$.

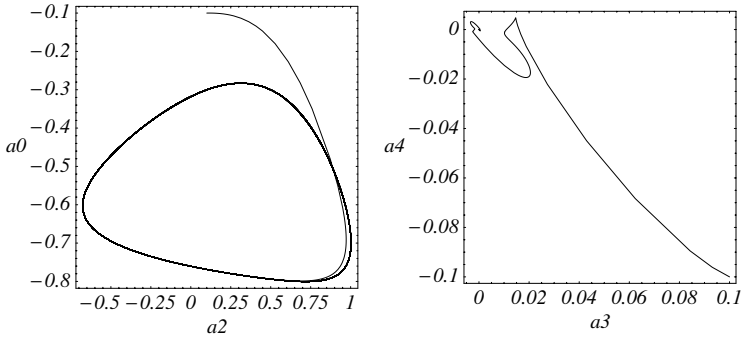

Figure 23. The orbit a_0 versus a_2 and the symmetry breaking orbit a_4 versus a_3 in the in-plane tumbling regime, at the shear rate 1.75 with the maximum shear deformation 1750. The temperature is $\vartheta = 0$; the model parameters are $\lambda_k = 1.25$ and $\kappa = 0$.

alignment tensor vanish in the long time limit as it is typical for in-plane periodic solutions. The component a_0 is also a periodic function oscillating about a constant, negative value. The

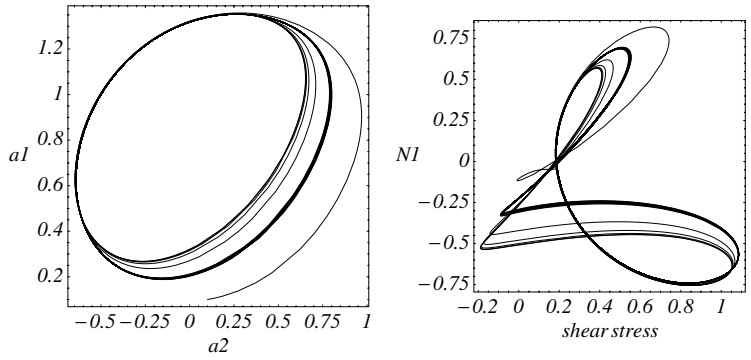

Figure 24. The in-plane orbit a_1 versus a_2 and the rheological phase portrait, namely the normal stress difference N_1 versus the shear stress in the kayaking–wagging regime, at the shear rate 1.82 with the maximum shear deformation 1820. The temperature is $\vartheta = 0$; the model parameters are $\lambda_k = 1.25$ and $\kappa = 0$.

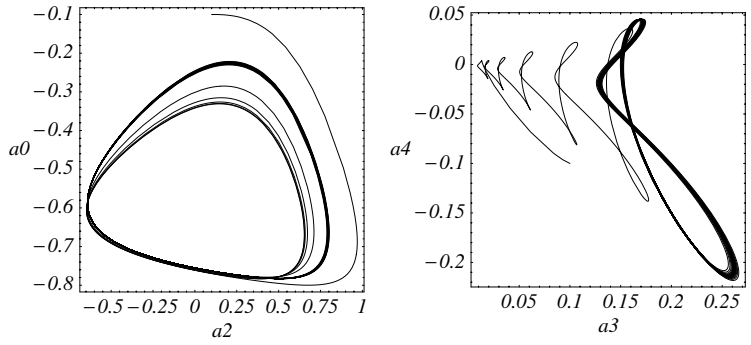

Figure 25. The orbit a_0 versus a_2 and the symmetry breaking orbit a_4 versus a_3 in the kayaking–wagging regime, at the shear rate 1.82 with the maximum shear deformation 1820. The temperature is $\vartheta = 0$; the model parameters are $\lambda_k = 1.25$ and $\kappa = 0$.

rheological phase portrait, namely the right graph of figure 22, looks more complex than the corresponding plot of a_1 versus a_2 for the alignment tensor. The instantaneous values of the first normal stress difference can be positive and rather large despite the fact that their time average yields a negative value. Also negative values occur for the shear stress during a small fraction of the periodic orbit. The time average of the shear stress is positive, and thus in accord with the second law.

4.4. Kayaking and wagging

For the model parameters under consideration, the KW type of dynamic behaviour occurs in a narrow range of shear rates slightly above 1.8. In figure 24 the in-plane orbit, namely the component a_1 of the alignment tensor versus a_2, and the rheological phase portrait are plotted for $\lambda_k = 1.25$ and $\kappa = 0$ at the temperature $\vartheta = 0$. The shear rate is $\dot{\gamma} = 1.82$. In figure 25 the orbits a_0 versus a_2 and a_4 versus a_3 are displayed. Notice that the asymptotic orbit of the symmetry breaking components a_3, a_4 does not enclose the point $a_3, a_4 = 0, 0$. This is a feature characteristic for the KW mode. It implies that the time average of these components is distinctively different from zero. Furthermore, the asymptotic state reached in the KW case

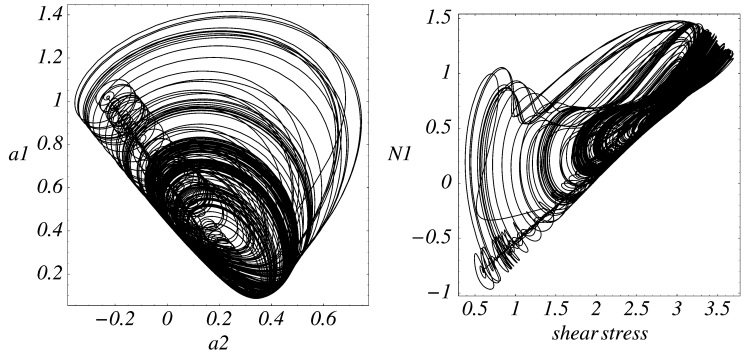

Figure 26. The in-plane orbit a_1 versus a_2 and the rheological phase portrait, namely the normal stress difference N_1 versus the shear stress in the chaotic regime, at the shear rate 3.75 with the maximum shear deformation 3750. The temperature is $\vartheta = 0$; the model parameters are $\lambda_k = 1.25$ and $\kappa = 0$.

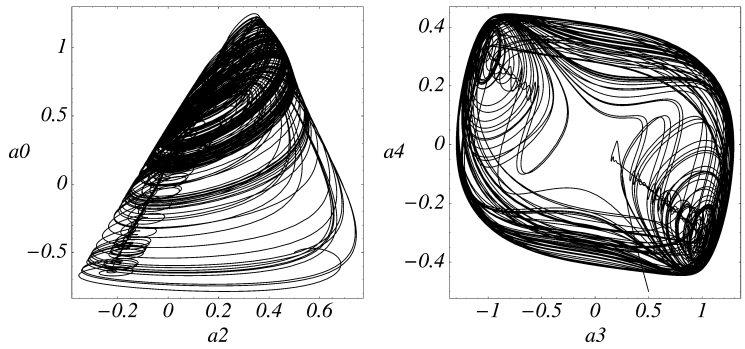

Figure 27. The orbit a_0 versus a_2 and the symmetry breaking orbit a_4 versus a_3 in the chaotic regime, at the shear rate 3.75 with the maximum shear deformation 3750. The temperature is $\vartheta = 0$; the model parameters are $\lambda_k = 1.25$ and $\kappa = 0$.

is not unique. Also the solutions with $-a_3$, $-a_4$ exist and will be attained from different initial conditions.

4.5. Chaotic behaviour

A stringent proof for a true chaotic behaviour does not follow from an inspection of the time dependence of the tensor components or of the phase portraits. However, it is instructive to compare the previous periodic asymptotic orbits with those for which it is known [13] from the computation of the Lyapunov exponents that the behaviour is chaotic. Examples for the alignment and the rheological properties are shown in figures 26 and 27.

Here orbits are shown for the case $\kappa = 0$ only. However, similar chaotic orbits and phase portraits also occur for non-zero κ, e.g. for $\vartheta = 0$, $\lambda_k = 1.05$, $\kappa = 0.4$ at the shear rate 4.2.

4.6. The flow aligned state at high shear rates

At high shear rates a flow aligned state is reached with orbits and rheological phase portraits which are rather simple compared with those shown above. For $\lambda_k = 1.25$, $\kappa = 0$ and $\lambda_k = 1.05$, $\kappa = 0.4$, at $\vartheta = 0$, this state is reached for shear rates above approximately 4.1

Table 1. Experimental data [4, 20] for the clearing temperature T_K (or concentration c_K), molecular weight M, length L, and width d of the axisymmetric ellipsoid model for p-methoxy-benzylidene-p-butylaniline (MBBA), octylcyanobiphenyl (8CB), tobacco mosaic (TMV) and polyethylene glycol coated fd virus (whose effective diameter for the calculation of p is 27 nm) [20, 21], together with theoretical estimates of the remaining quantities for given temperature and density (ρ, T or T, c). For the table, a reduced 'temperature' $\vartheta = 1/2$ and $\delta_K = 1/100$ are assumed. Therefore, we consider pseudo-critical temperatures $T^* = (1 - \delta_K)T_K = 0.99T_K$, samples at temperatures $T = (T_K/\vartheta)(\vartheta - \delta_K)/(1 - \delta_K) \approx 0.9899T_K$, and an order parameter $S_2 \approx 1.3S_K \approx 0.42$; see section 5 for further details and definitions. An axis ratio $p = 0.7L/d$ (the approximate result for cylinders) rather than $p = L/d$ (for ellipsoids) was used, and water ($\eta_s = 0.1$ mPa s) has been used as a solvent for evaluating sample values. The experimental viscosities, relaxation times, order parameters etc differ by less than a factor of two from the values predicted here.

	T_K (K)	M (g mol^{-1})	ρ, T (g ml^{-1}, K)	$L/d/p$ (Å/Å/)	R (Å)	κ	e_r	λ_k	λ_{eq}	η (mPa s)	τ_{ref} (10^{-6} s)
MBBA	317	300	1, 314	45/6/5.3	0.930	0.40	5.0	1.16	1.02	85	2.3
8CB	313	278	1, 310	29/3.6/5.6	0.939	0.40	5.5	1.17	1.03	24	0.6
	c_K (mg ml^{-1})	M (10^7 g mol^{-1})	T, c (K, mg ml^{-1})	$L/d/p$ (nm/nm/)	R (Å)	κ	e_r	λ_k	λ_{eq}	η (mPa s)	τ_{ref} (s)
fd virus	11	1.6	300, 10.9	880/9/23	0.996	0.43	53	1.24	1.09	6.8	1.2
TMV	20	4	300, 19.8	300/18/17	0.985	0.42	17	1.22	1.08	4.6	0.9

and 4.3, respectively. The first normal stress difference is negative, whereas it is positive in the non-tumbling nematics.

5. Model parameters for specific fluids

The following remarks are intended to give some hints as regards the application of the theory to specific molecular fluids and colloidal dispersions. As mentioned before, the model parameters can be related 'molecular' properties by using a mesoscopic theory starting from a generalized Fokker–Planck equation [6, 17, 31]. For ellipsoids of revolution with the semi-axes a, $b = a$, c and the axis ratio $p = c/a$, one has $\lambda_k = (2/\sqrt{5}a_K)R = 2R/(5S_K)$, $\kappa = (3/7)R$ with the 'shape factor' R given by $R = (p^2 - 1)/(p^2 + 1)$. Some guidance for the application of these formulae is given through table 1. Here S_K is the equilibrium value of the Maier–Saupe order parameter at the transition to the nematic phase. The quantity R vanishes for spherical particles corresponding to $p = 1$; it approaches the values 1 and -1 for very thin rods and discs, respectively. The specific expression for R was inferred from hydrodynamics [32], applicable to larger particles in dilute suspensions. For molecular fluids, experimental data indicate that R is slightly larger than 1 [42]. Thus for practical purposes, it seems appropriate to determine the model parameter λ_k either from the flow birefringence in the isotropic phase—see section 3.2—or from the value of the tumbling parameter via the flow alignment angle, at small shear rates, just inside the nematic phase.

To find the chaotic domain for tumbling nematics one needs the reference value τ_{ref} for the time—see (11); for the shear rate the reference value is τ_{ref}^{-1}. From mesoscopic theory one can obtain values for this quantity subject to certain approximations. For example, one expects $\tau_{ref} = \tau_a\delta_K^{-1}$ with $\tau_a = \eta_s V/(k_B T)e_r$, where η_s is the solvent viscosity, V the volume of a single dissolved molecule, and e_r is another shape factor which becomes $e_r = 2p^2/(3(2\ln(2p) - 1))$ for $p \gg 1$ and $e_r = 1 + \epsilon/5$ for $p = 1 + \epsilon$, $|\epsilon| \ll 1$ [38]. The contribution to the viscosity is of the order of $\eta \approx \nu k_B T \tau_a$, where ν denotes the number density of the molecules (the precise expression in terms of particle shape is given in [38]). These relationships are used in

table 1. Again, it seems advisable to infer this quantity directly from experiments, e.g. from the dependence of the flow angle on the shear rate in the isotropic phase—see (26)—or, in the nematic phase, from the Jeffrey tumbling period P_J. For $|\lambda_{eq}| < 1$ and in the limit of small shear rates $\dot{\gamma}$, the Jeffrey tumbling period [23] is related to the Ericksen–Leslie tumbling parameter λ_{eq} by $P_J = 4\pi/(\dot{\gamma}\sqrt{1-\lambda_{eq}^2})$, for a full rotation of the director. Strictly speaking, this expression applies to in-plane tumbling at small shear rates. It also gives a good estimate for half of the tumbling period of the components a_1 and a_2 of the alignment tensor in the kayaking–tumbling regime [13]. For the symmetry breaking components the periodicity is approximately determined by the full tumbling period P_J. For the state point $\vartheta = 0$ and $\lambda_{eq} = 5/6$, as studied here in some detail, the chaotic regime is close to the dimensionless shear rate $\dot{\gamma} \approx 4$ corresponding to $P_J \approx 1.8\pi \approx 5.7$.

6. Conclusions

In this paper, results are presented for the rheological behaviour and for the underlying dynamics of the alignment of tumbling nematic liquid crystals. The basic theory is outlined. For selected state points and model parameters, rheological properties, orbits, and phase portraits are displayed graphically, as obtained from numerical solutions of the relevant equations (20)–(23). The analysis was restricted to a situation with a spatially homogeneous velocity gradient as in an ideal plane Couette flow. In general, one has to deal with a spatially inhomogeneous alignment and with the onset of a secondary flow, as is typical for a non-Newtonian fluid. Thus the equation for the alignment tensor has to be amended and the full hydrodynamic problem has to be solved. The first issue is related to the tensorial treatment [43] of the Frank elasticity of nematics. In the one-coefficient approximation, this requires an additional term [14] $-\ell^2\Delta\boldsymbol{a}$, with a characteristic length ℓ, on the left-hand side of (2); see also [22]. For the second task, it is desirable to apply and test, in addition to grid based methods, smooth particle and dissipative particle methods in the spirit of [44]; i.e., the stress and alignment tensors should be used as local dynamic variables. The tensorial rheological model used in [45] to treat fluids which show both shear thinning and shear thickening is also expected to imply chaotic behaviour, which deserves a similar analysis. Furthermore, it seems feasible to treat the shear flow induced changes seen in side chain polymeric liquids [41] with a two-alignment tensor theory, one tensor specifying the alignment of the mesogenic side groups, the other one characterizing the orientation of the backbone. On the other hand, in lyotropic liquid crystals, the coupling between the alignment tensor and changes of the local concentration [19, 22] may play an important role. The dynamics of these systems is expected to be even more complex than that detected and analysed so far.

Acknowledgments

This research is the follow-up of a project which was supported in part by the National Science Foundation under grant No PHY99-07949 via the programme ‘Dynamics of complex and macromolecular fluids’ at the ITP, Santa Barbara, and it has been performed under the auspices of the Sonderforschungsbereich 448 ‘Mesoskopisch strukturierte Verbundsysteme’ (Deutsche Forschungsgemeinschaft).

References

[1] Ericksen J L 1961 *Trans. Soc. Rheol.* **5** 23
Leslie F M 1968 *Arch. Ration. Mech. Anal.* **28** 265

[2] de Gennes P G 1974 *The Physics of Liquid Crystals* (Oxford: Clarendon)
[3] Kelker H and Hatz R 1980 *Handbook of Liquid Crystals* (Weinheim: Verlag Chemie)
[4] Larson R G 1999 *The Structure and Rheology of Complex Fluids* (Oxford: Oxford University Press)
[5] Hess S 1975 *Z. Naturf.* a **30** 728
[6] Hess S 1976 *Z. Naturf.* a **31** 1034
[7] Gähwiler C 1972 *Phys. Rev. Lett.* **28** 1554
Pieranski P and Guyon E 1974 *Phys. Rev. Lett.* **32** 924
[8] Kiss G and Porter R S 1978 *J. Polym. Sci. Polym. Symp.* **65** 193
Moldenaers P and Mewis J 1986 *J. Rheol.* **30** 567
Mewis J, Mortimer M, Vermant J and Moldenaers P 1997 *Macromolecules* **30** 1323
[9] Fischer P 2000 *Rheol. Acta* **39** 234
[10] Schmitt V, Lequeux F, Pousse A and Roux D 1994 *Langmuir* **10** 955
Wunenburger A S, Colin A, Leng J, Arnedeo A and Roux D 2001 *Phys. Rev. Lett.* **86** 1374
Berret J F, Roux D C, Porte G and Lindner P 2002 *Europhys. Lett.* **25** 521
[11] Rienäcker G 2000 Orientational dynamics of nematic liquid crystals in a shear flow *Thesis TU Berlin 2000* (Aachen: Shaker Verlag)
[12] Grosso M, Keunings R, Crescitelli S and Maffettone P L 2001 *Phys. Rev. Lett.* **86** 3184
[13] Rienäcker G, Kröger M and Hess S 2002 *Phys. Rev.* E **66** 040702(R)
Rienäcker G, Kröger M and Hess S 2002 *Physica* A **315** 537
[14] Hess S and Pardowitz I 1981 *Z. Naturf.* a **36** 554
[15] Pereira Borgmeyer C and Hess S 1995 *J. Non-Equilib. Thermodyn.* **20** 359
[16] Hess S 1979 Flow alignment of a colloidal solution which can undergo a transition from the isotropic to the nematic phase (liquid crystal) *Electro-Optics and Dielectrics of Macromolecules and Colloids* ed B R Jennings (New York: Plenum)
[17] Doi M 1980 *Ferroelectrics* **30** 247
Doi M 1981 *J. Polym. Sci. Polym. Phys. Edn* **19** 229
[18] Bandyopadhyay R, Basappa G and Sood A K 2000 *Phys. Rev. Lett.* **84** 2022
Bandyopadhyay R and Sood A K 2001 *Europhys. Lett.* **56** 447
[19] Cates M E, Head D A and Ajdari A 2002 *Phys. Rev.* E **66** 025202
[20] Vroege G J and Lekkerkerker H N W 1992 *Rep. Prog. Phys.* **55** 1241
Dogic Z and Fraden S 2001 *Phil. Trans. R. Soc.* A **359** 997
Purdy K R, Dogic Z, Fraden S, Ruhm A, Lurio L and Mochrie S G J 2003 *Phys. Rev.* E **67** 031708
[21] Lettinga M P, Dogic Z, Vermant J and Dhont J K G 2003 Dynamic behaviour of liquid crystalline fd-virus suspensions in shear *AERC2003, Program and Abstracts* ed J Maia and J Covas (Guimaraes: European Society of Rheology) p 81 (see also contribution by Lettinga *et al* in this issue)
[22] Forest M G, Wang Q and Zhou R 2004 *Rheol. Acta* **43** 17
Fielding S M and Olmsted P D 2004 *Phys. Rev. Lett.* **92** 084502
Chakrabarti B, Das M, Dasgupta C, Ramaswamy S and Sood A K 2004 *Phys. Rev. Lett.* **92** 055501
[23] Jeffrey G B 1922 *Proc. R. Soc.* A **102** 171
[24] Hess S 1976 *Z. Naturf.* a **31** 1507
[25] Olmsted P D and Goldbart P 1990 *Phys. Rev.* A **41** 4578
Olmsted P D and Goldbart P 1992 *Phys. Rev.* A **46** 4966
[26] Marrucci G 1991 *Macromolecules* **24** 4176
Marrucci G and Maffettone P L 1989 *Macromolecules* **22** 4076
Marrucci G and Maffettone P L 1990 *J. Rheol.* **34** 1217
Maffettone P L, Sonnet A and Virga E G 2000 *J. Non-Newton. Fluid Mech.* **90** 283
Maffettone P L and Crescitelli S 1995 *J. Non-Newton. Fluid Mech.* **59** 73
Maffettone P L and Crescitelli S 1994 *J. Rheol.* **38** 1559
Farhoudi Y and Rey A D 1993 *J. Rheol.* **37** 289
Wang Q 1997 *J. Rheol.* **41** 943
Andrews N C, McHugh A J and Edwards B J 1996 *J. Rheol.* **40** 459
Ilg P, Karlin I V, Kröger M and Öttinger H C 2003 *Physica* A **319** 134
Dhont J K G and Briel W J 2003 *Colloids Surf.* A **213** 131
[27] Feng J, Chaubal C V and Leal L G 1998 *J. Rheol.* **42** 1095
[28] Forest M G, Zhou R and Wang Q 2003 *J. Rheol.* **47** 105
[29] Rienäcker G and Hess S 1999 *Physica* A **267** 294
[30] Chillingworth D R J, Alonso E V and Wheeler A A 2001 *J. Phys. A: Math. Gen.* **34** 1393
[31] Kröger M 2004 *Phys. Rep.* **390** 453

[32] Peterlin A and Stuart H A 1943 *Hand- und Jahrbuch der Chemischen Physik* vol 8, ed Eucken-Wolf (Leipzig: Akademische Verlagsgesellschaft) p 113
[33] Zannoni C 2000 Liquid crystal observables: static and dynamic properties *Advances in the Computer Simulations of Liquid Crystals* ed P Pasini and C Zannoni (Dordrecht: Kluwer–Academic)
[34] Muschik W, Ehrentraut H and Papenfuss C 1997 *J. Non-Equilib. Thermodyn.* **22** 285
Muschik W and Su B 1997 *J. Chem. Phys.* **107** 580
[35] Fuller G G 1995 *Optical Rheometry of Complex Fluids* (New York: Oxford University Press)
[36] Marrucci G and Greco F 1991 *Mol. Cryst. Liq. Cryst.* **206** 17
Kröger M and Sellers H S 1992 *Complex Fluids* (*Springer Lecture Notes in Physics* vol 415) ed L Garrido (New York: Springer) pp 295–301
Sgalari G, Leal G L and Feng J J 2002 *J. Non-Newton. Fluid Mech.* **102** 361
Dhont J K G and Briel W J 2003 *J. Chem. Phys.* **118** 1466
[37] Schneggenburger C, Kröger M and Hess S 1996 *J. Non-Newton. Fluid Mech.* **62** 235
[38] Kröger M and Sellers H S 1995 *J. Chem. Phys.* **103** 807
[39] Kaiser P, Wiese W and Hess S 1992 *J. Non-Equilib. Thermodyn.* **17** 153
[40] Hess S and Kröger M 2004 *Computer Simulations Bridging Liquid Crystals and Polymers* ed P Pasini, C Zannoni and S Zumer (Dordrecht: Kluwer–Academic)
[41] Pujolle-Robic C, Olmsted P D and Noirez L 2002 *Europhys. Lett.* **59** 364
[42] Vermant J, Yang H and Fuller G G 2001 *AIChE J.* **47** 790
[43] Pardowitz I and Hess S 1980 *J. Chem. Phys.* **76** 1485
[44] Ellero M, Kröger M and Hess S 2002 *J. Non-Newton. Fluid Mech.* **105** 35
[45] Hess O and Hess S 1994 *Physica* A **207** 517